Polymer Chemistry

RSC Publishing

PAPER

View Article Online
View Journal | View Issue

Orderly arranged NLO materials on exfoliated layered templates based on dendrons with alternating moieties at the periphery†

Cite this: *Polym. Chem.*, 2013, **4**, 2747

Ya-Yu Siao,[a] Shi-Min Shau,[a] Wei-Hsiang Tsai,[a] Yung-Chung Chen,[a] Tain-Hao Wu,[a] Jiang-Jen Lin,[b] Tzong-Ming Wu,[a] Rong-Ho Lee*[a] and Ru-Jong Jeng*[b]

Received 8th January 2013
Accepted 12th February 2013

DOI: 10.1039/c3py00034f

www.rsc.org/polymers

Nonlinear optical dendrons with alternating terminal groups of the stearyl group (C18) and chromophore were prepared through a convergent approach. These chromophore-containing dendrons were used as the intercalating agents for montmorillonite *via* an ion-exchange process. An orderly exfoliated morphology is obtained by mixing the dendritic structure intercalated layered silicates with a polyimide. As a result, optical nonlinearity, *i.e.* the Pockels effect was observed for these nanocomposites without resorting to the poling process. EO coefficients of 9–22 pm V^{-1} were achieved despite that relatively low NLO densities were present in the nanocomposites, particularly for the samples comprising the dendrons with alternating moieties. In addition, the hedging effects of the stearyl group on the self-alignment behavior, electro-optical (EO) coefficient and temporal stability of the dendron-intercalated montmorillonite/polyimide nanocomposites were also investigated.

1 Introduction

Second-order nonlinear optical (NLO) polymers have attracted much attention because of their potential applications, such as optical waveguides, modulators to transfer data into optical waves, low-power wavelength conversion and tuning, and optical switching.[1–5] In general, second-order NLO properties are present in the polymers when the NLO chromophores are aligned in a noncentrosymmetric manner *via* a poling technique.[3–7] Large second-order NLO coefficient and excellent temporal stability are required for the above-mentioned applications. In order to meet these requirements, a large amount of NLO-active chromophores are usually incorporated into the polymer with a high glass transition temperature (T_g).[8,9] However, strong dipolar interactions would restrict the alignment efficiency of the NLO chromophores in the polymer and consequently result in poor Pockels effect, *i.e.* small electro-optical (EO) coefficients.[8–10] In addition, molecular relaxation of the polymer chains is detrimental to the orientational degree of the NLO chromophores.[11,12]

NLO-active dendritic structure-containing polymers with site isolation effects have been of great interest recently.[13–18] Jen and Ma reported that the NLO-active chromophores can be incorporated into the periphery, branch, or core of a dendrimer to construct precise molecular architecture with enhanced NLO performance.[13] The poled film based on the dendronized chromophores with a relatively low NLO density exhibited a larger EO coefficient than that of the sample based on typical chromophores with a higher NLO density.[14] The large enhancement of the EO coefficient in a poled dendrimer is mainly due to the dendritic site-isolation effect that reduces electrostatic interactions among the chromophores. Do *et al.* reported that the global-like dendrimers prepared *via* "click chemistry" reaction exhibited large r_{33} values (43.4 pm V^{-1}) due to the presence of a three-dimensional (3D) structure and isolation effect.[16] In addition, we reported polyimides doped with a series of chromophore-containing dendrons.[18] The site isolation effects derived from the dendrons did enhance the NLO properties, especially the sample with higher generation of dendrons.

In order to preserve the NLO properties, the randomization of the poled NLO chromophore has to be prevented by all means. Therefore, various strategies have been devised to achieve polar order without resorting to electric poling, which include Langmuir–Blodgett (LB) growth, molecular self-assembly, *etc.*[19–22] However, the problem of limited long-term NLO stability at elevated temperatures is still present in these systems. Recently, the assembly behaviors of organic molecules on the layered silicates such as montmorillonite (MMT) were investigated.[23–28] The conformations of organic molecules on MMT platelets were affected by the anchoring role of the polar head groups and the hydrophobicity of peripheral groups, cationic exchange capacity

[a]*Department of Chemical Engineering, National Chung Hsing University, Taichung 402, Taiwan. E-mail: rhl@nchu.edu.tw; Fax: +886-4-22854734; Tel: +886-4-22854308*
[b]*Institute of Polymer Science and Engineering, National Taiwan University, Taipei 10617, Taiwan. E-mail: rujong@ntu.edu.tw; Fax: +886-2-33665237; Tel: +886-2-33665884*

† Electronic supplementary information (ESI) available. See DOI: 10.1039/c3py00034f

(CEC) equivalents, and temperature control of the intercalation procedure.[23–28] More recently, we modified the surface of MMT using a series of hydrogen bond-rich polyurea(urethane)/malonamide dendrons consisting of disperse red 1 (DR1) chromophores at the periphery.[29,30] Using 4-isocyanato-4′(3,3-dimethylazetidine-2,4-dione)diphenylmethane (IDD) based dendrons comprising a secondary amine functional group in the focal point as the intercalating agents allowed the preparation of dendron/MMT nanohybrids that revealed intercalated and exfoliated morphology. The modified organoclay sample with bulky dendrons exhibited an ordered morphology and subsequently NLO properties without applying the poling process. The self-organized behavior of the chromophore-containing dendrons on the exfoliated layered silicates was studied. Moreover, a polyimide with a high T_g was introduced as the host not only to improve thin film formability, but to provide interaction-induced orientation toward dendrons as well.

In this study, a series of NLO-active dendrons with alternating peripheral moieties were synthesized for second-order nonlinear optics. The chromophore-containing dendrons were prepared based on two different building blocks, IDD and 1-(4-isocyanatophenyl)-3,3-dimethylazetidine-2,4-dione (IPDA). These dendrons with peripheral DR1 chromophores or alternating moieties of the stearyl group (C18) and the DR1 chromophore at the periphery were prepared through a convergent approach. Due to the presence of the methylene group situated between the two aromatic rings, the IDD based dendritic structure is kinked and the NLO-active moieties might rotate freely around the $-CH_2-$ moiety, which would cause the disruption of planar symmetry and ordered packing of the dendritic structures. Therefore, the IPDA building block was utilized to construct a new series of dendrons to circumvent the above-mentioned drawbacks. In addition, the alternating C18 group and DR1 chromophore were introduced onto the periphery of dendrons. Long alkyl chain groups, *i.e.* C18, were used as molecular hedges to completely prevent dipolar interactions among chromophores. This would not only solve the chromophore aggregation problem but also enhance the non-centrosymmetric alignment. Furthermore, the NLO-active dendrons consisting of secondary amines in the focal points were acidified to form the amine salts, and then utilized to intercalate into Na^+-MMT *via* an ion-exchange process. The morphology of the dendron intercalated MMTs was confirmed by the TEM and X-ray diffraction patterns. Taking film formability and NLO temporal stability into account, the NLO-active dendron intercalated MMTs were further blended with a polyimide. The steric bulkiness of the dendritic structures and the interaction between the layered silicates and ITO glass substrates would bring about an ordered morphology, leading to the realization of NLO properties.

2 Experimental

2.1 Materials

Isobutyryl chloride, triethylamine (TEA), methylene di-*para*-phenyl isocyanate (MDI), diethyltriamine (DETA), and stearyl alcohol (C18–OH) were purchased from Sigma-Aldrich and Acros Co. Compound 1,4-phenylene diisocyanate (PDI) was purchased from TEDIA. All chemicals were used as received unless otherwise stated. Disperse Red 1 (DR1, purchased from Lancaster) was purified from acetone before use. Na^+-MMT supplied by Nanocor Co. is a sodium type with a cationic exchange capacity (CEC) of 1.20 mequiv. g^{-1} and a surface area of 750 m^2 g^{-1}. *N*,*N*-Dimethylacetamide (DMAc), *N*,*N*-dimethylformamide (DMF), tetrahydrofuran (THF), dimethyl sulfoxide (DMSO), 1,4-dioxane, xylene, acetone, methanol, ethylene acetate (EA), cyclohexane, hexane *etc.* were obtained from Tedia Chemical Co. All reagents and solvents are of reagent grade. DMAc and DMF were purified through distillation under reduced pressure over CaH_2 and then stored over 4 Å molecular sieves. THF was distilled under nitrogen from sodium/benzophenone before use. The IDD- and IPDA-based dendrons with peripheral DR1 chromophores or alternating moieties of the stearyl group (C18) and the DR1 chromophore at the periphery were synthesized according to Schemes 1 and 2. The dendrons with peripheral DR1 molecules are identified with symbols in the form "D-G(*X*)-DR1 and A-G(*X*)-DR1", where D refers to the building block IDD, A refers to the building block IPDA, G(*X*) denotes the generation number of the dendrons (from G0.5 to G3); DR1 refers to the peripheral groups of the NLO chromophore DR1. The dendrons with alternating peripheral groups of C18 and DR1 are identified with symbols in the form "D-G(*X*)-CD and A-G(*X*)-CD", where CD refers to the alternating peripheral C18 groups and DR1 molecules. The building block IDD, dendrons D-G0.5-DR1–D-G3-DR1 and D-G0.5-C18 were synthesized according to the procedure in our previous study.[18,29,31] Synthetic procedures of the building block IPDA, dendrons A-G0.5-DR1–A-G3-DR1, D-G0.5-CD–D-G3-CD, and A-G0.5-CD–A-G3-CD are shown in the ESI.†

2.2 Preparation of DR1 containing dendron intercalated MMTs

According to our previous studies,[29,30] MMTs could be intercalated with the DR1 containing dendrons with integer generation. Typical experimental procedures for preparing the organo-modified MMTs are described below. Na^+-MMT (2.00 g, 2.40 equiv. kg^{-1}) and deionized water (150 mL) were stirred vigorously in a 250 mL flask at 80 °C for 3–4 h until fully swollen. In a separate vessel, the as-prepared dendron with the same equivalent of Na^+-MMT dissolved in DMAc (20 mL) was acidified with hydrochloric acid (37% in water, 0.234 g, 2.40 mmol). The solution of the acidified intercalating agent was poured into the flask containing the Na^+-MMT slurry; the ensuing mixture was stirred vigorously at 80 °C for 4 h and then it was cooled to room temperature. The resulting agglomerated precipitate was collected and washed sequentially with water and acetone (twice) to remove any residual ions or free intercalating agents. The dendron intercalated MMT materials were obtained after drying in a vacuum oven at 80 °C for 24 h.

2.3 Characterizations

^1H NMR spectra were taken on a Varian Gemini-400 FT-NMR spectrometer with $CDCl_3$ and d-DMSO. Fourier transform

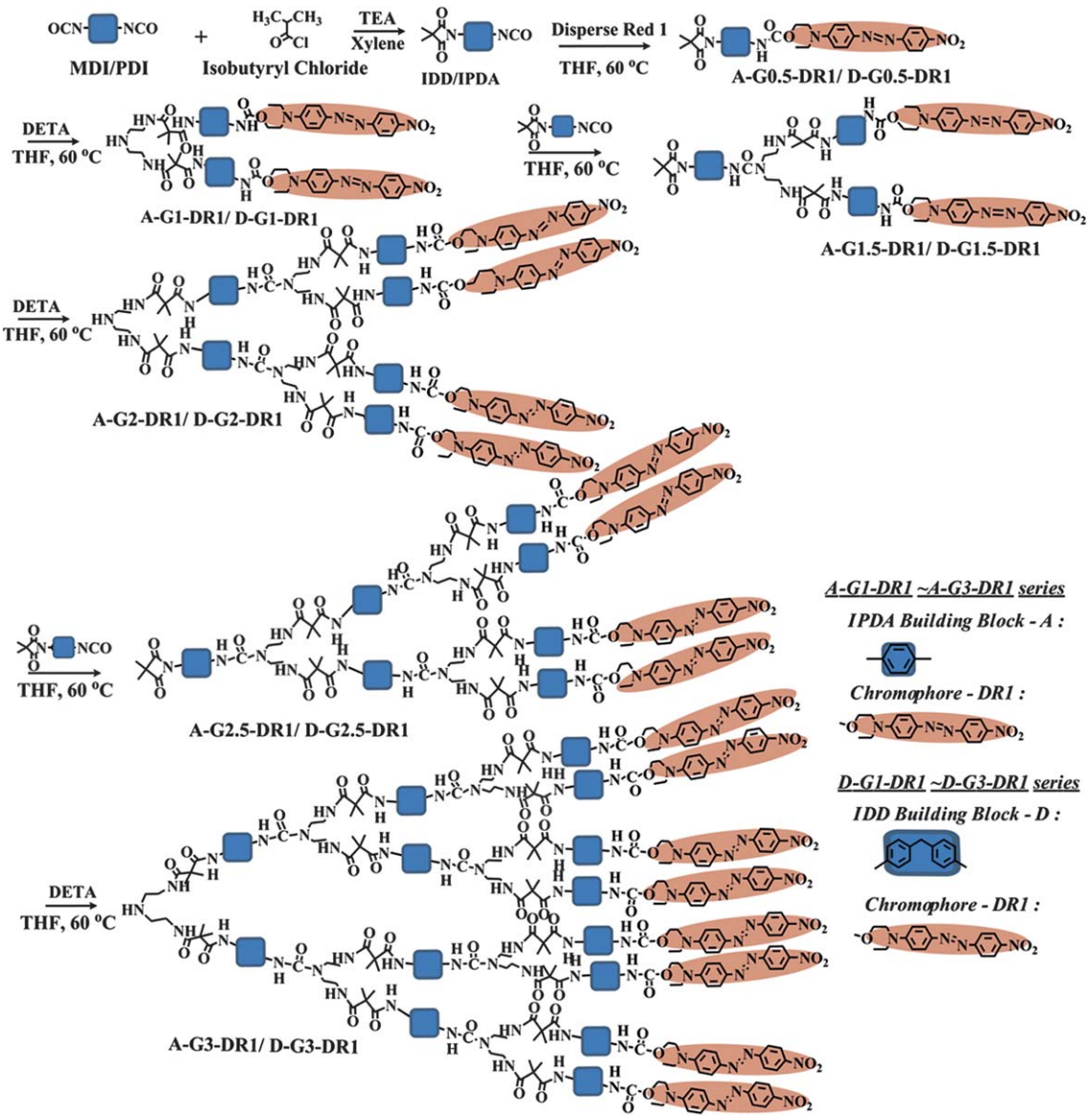

Scheme 1 Synthesis of IPDA and IDD building block based dendrons (A-G1-DR1–A-G3-DR1 and D-G1-DR1–D-G3-DR1) with peripheral DR1 chromophores.

infrared (FTIR) spectrum measurement was performed on a HORIBA FT-720 FTIR spectrometer. Elemental analysis was performed on a Heraeus CHNOS Rapid Analyzer. Thermal analysis was performed in N_2 on a Seiko DSC 6220 (S|| EXATAR 6000) at a heating rate of 10 °C min^{-1}. Glass transition temperatures (T_gs) of the dendrons were measured using a differential scanning calorimeter (DSC, Sekio SSC-5200). Thermal degradation temperatures (T_ds) were measured using a Thermo Cahn Versa thermogravimetric analyzer (TGA) at a heating rate of 10 °C min^{-1} under nitrogen. Fast atom bombardment mass spectrometry (FAB MS) analysis was performed on a JEOL JMS SX/SX 102A mass spectrometer equipped with the standard FAB. Matrix-assisted laser desorption ionization with time of flight (MALDI-TOF) mass spectra were recorded on a Voyager DE-PRO (Applied Biosystems, Houston, TX) equipped with a nitrogen laser (337 nm) operating in linear detection mode to generate positive ion spectra with dithranol as a matrix, DMSO as a solvent, and sodium trifluoroacetate as an additive agent. The *d*-spacing of the dendron intercalated MMTs was analyzed using an X-ray powder diffractometer (XRD, Shimadzu SD-D1 using a Cu target at 35 kV, 30 mA). The *d*-spacing of the dendron intercalated MMTs was calculated by using Bragg's equation ($n = 2d\sin\theta$). Transmission electron microscopy (TEM) was performed on a Zeiss EM 902A and operated at 80 kV.

2.4 Thin film preparation and EO measurements

A polyimide (PI; T_g = 270 °C) based on 2,2-bis(3-amino-4-hydroxyphenyl)hexafluoropropane and 4,4′-oxydiphthalic dianhydride was synthesized for its use as a polymer host for NLO-active dendron-MMT/PI nanocomposites.[18] The NLO-active dendron-MMT/PI nanocomposites were prepared by mixing the polyimide with 10 wt% and 20 wt% of the DR1

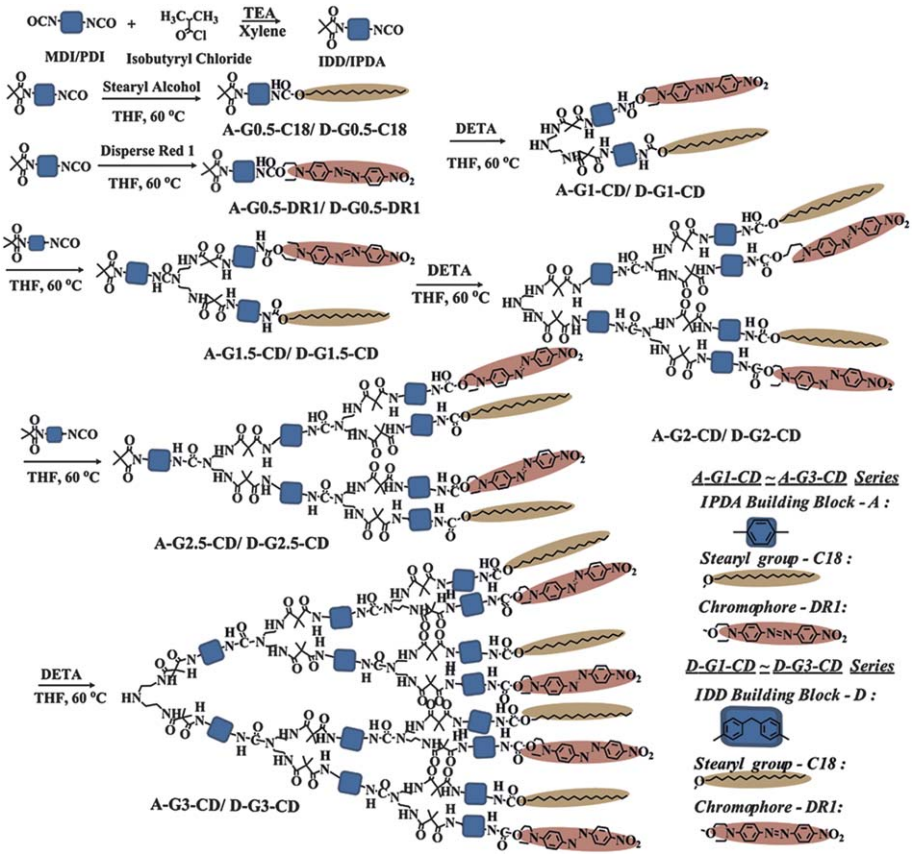

Scheme 2 Synthesis of IPDA and IDD based dendrons (A-G1-CD–A-G3-CD and D-G1-CD–D-G3-CD) with alternating terminal groups of DR1 and alkyl chain C18.

containing dendron-MMT materials in DMAc, respectively. The dendron-MMT–polyimide solution was then cast onto indium-tin-oxide (ITO) glass substrates. The NLO-active polymer film was dried at 60 °C in a vacuum oven for 6 h to ensure the removal of any residual solvent. It is important to note that the polyimide was introduced as the polymer host not only for further exfoliation, but also for imparting film formability and quality as well. A thin layer of silver was sputtered onto the films as a top electrode for EO measurement. EO coefficients (r_{33}) were measured by a simple reflection technique.[29,30]

3 Results and discussion

3.1 Characterization of chemical structures and physical properties of the NLO-active dendrons

The new building block IPDA was prepared *via* the same convergent synthetic strategy as that of IDD (Scheme 1). The DR1 containing dendrons based on IPDA with various generations (A-G0.5-DR1 to A-G3-DR1) were synthesized by the addition reaction of IPDA and DR1. For example, A-G0.5-DR1 was synthesized by the addition reaction between the isocyanate group of IPDA and the hydroxyl group of DR1. Malonamide linkages in the dendrons were formed based on the facile ring-opening addition reactions of azetidine-2,4-dione with the aliphatic primary amine group. In addition, the synthesis routes of the building block IDD or IPDA based dendrons with alternating terminal groups of C18 and DR1 are shown in Scheme 2. A-G1-CD was readily obtained by the ring-opening addition reaction of the azetidine-2,4-dione group of A-G0.5-C18 and A-G0.5-DR1 toward the aliphatic amines of DETA. This is because the azetidine-2,4-dione containing A-G0.5-C18 and A-G0.5-DR1 dendrons react only with the aliphatic primary amine groups, but not with the secondary amine at the center of DETA. The functional group of the secondary amine located at the focal point of A-G1-CD became the next reaction site for IPDA. After sequential and alternative incorporations of IPDA and DETA into the various growing dendrons, IPDA based dendrons with different generations were obtained.

Fig. 1(a) shows the FTIR spectra of A-G1.5-DR1, D-G1.5-CD, and A-G1.5-CD. For these dendrons, the isocyanate group (2260 cm^{-1}) of IDD or IPDA was absent, whereas the absorption peaks of nitro groups (1516 and 1334 cm^{-1}) were observed. The absorption peaks of the azetidine-2,4-dione groups (1855 and 1740 cm^{-1}) in these samples were still intact. Moreover, higher absorption intensity of alkyl chains (2750–3000 cm^{-1}) was observed for D-G1.5-CD and A-G1.5-CD as compared to that of A-G1.5-DR1. FTIR spectra of A-G2-DR1, D-G2-CD, and A-G2-CD are shown in Fig. 1(b). The inward coupling reaction was begun by the ring-opening addition reaction of generation 1.5 (G1.5) dendrons toward DETA to give generation 2 (G2) dendrons with a secondary amine at the focal point. The absorption peaks at 1855 and 1740 cm^{-1} disappeared completely after the coupling reaction. This indicates that the ring-opening addition reaction was rapidly displaced by the emergence of a new absorption

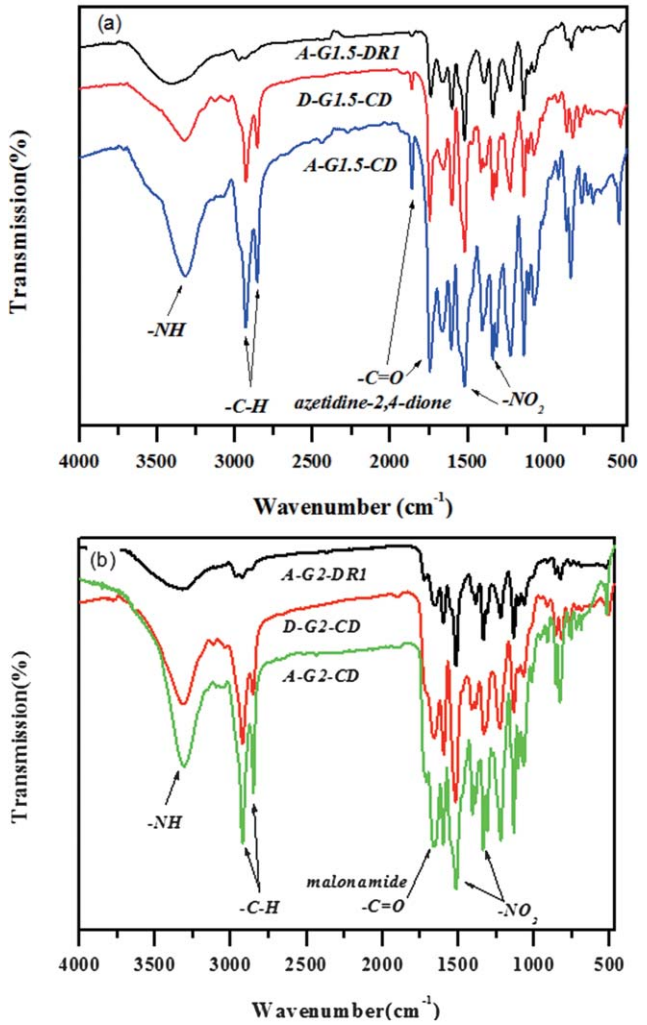

Fig. 1 FTIR spectra of the NLO-active dendrons.

peak at 1664 cm^{-1} corresponding to the carbonyl group of the malonamide linkage. Furthermore, ^{1}H-NMR spectra are in good agreement with the structures of dendron molecules. The results of elemental analysis of the dendrons were also close to those calculated. Apart from that, MALDI-TOF-MS was also employed for the determination of molecular weights (Table 1), which are in agreement with the calculated ones.

T_gs and T_ds of the dendrons are summarized in Table 1. The dendron D-G1-CD exhibited a T_m and T_g at 138 and 82 °C, respectively. This G1 dendron is ready to extend in linear shape and consequently to form highly ordered packing.[32] However, the rest of the dendrons were amorphous exhibiting only T_gs that ranged from 50 °C to 92 °C. The lack of crystallinity is attributed to the disruption of molecular packing due to the highly branched structure of the dendrons. For the IPDA based dendrons with peripheral DR1 molecules (A-G(X)-DR1), the T_g increased with increasing molecular weight and generation of dendron. A highest T_g of 92 °C was observed for A-G2.5-DR1. However, the T_g of A-G3-DR1 was 25 °C lower than that of A-G2.5-DR1. This might be possibly caused by the difficult molecular packing because of its highly branched nature as the

Table 1 Characteristics and thermal properties of the NLO-active dendrons

Sample	Formula/M_w	Yield (%)	M_w[a]	T_m[b]	T_g[b]	T_d[c]
A-G1-DR1	$C_{60}H_{69}N_{15}O_{12}$/1192.28	65%	1192	n.a.[d]	76	239
A-G1.5-DR1	$C_{72}H_{79}N_{17}O_{15}$/1422.50	57%	1422	n.a.	82	244
A-G2-DR1	$C_{148}H_{171}N_{37}O_{30}$/2948.17	54%	2971	n.a.	89	227
A-G2.5-DR1	$C_{160}H_{181}N_{39}O_{33}$/3178.00	35%	3201	n.a.	92	242
A-G3-DR1	$C_{324}H_{375}N_{81}O_{66}$/6459.95	33%	6483	n.a.	67	194
D-G1-CD	$C_{76}H_{101}N_{11}O_{10}$/1328.68	65%	1329	138	82	238
D-G1.5-CD	$C_{95}H_{117}N_{13}O_{13}$/1649.02	36%	1649	n.a.	52	279
D-G2-CD	$C_{194}H_{247}N_{29}O_{26}$/3401.22	37%	3401	n.a.	58	256
D-G2.5-CD	$C_{213}H_{263}N_{31}O_{29}$/3721.56	71%	3721	n.a.	60	256
D-G3-CD	$C_{430}H_{539}N_{65}O_{58}$/7546.28	31%	7546	n.a.	58	205
A-G1-CD	$C_{62}H_{89}N_{11}O_{10}$/1148.44	65%	1148	n.a.	50	239
A-G1.5-CD	$C_{74}H_{99}N_{13}O_{13}$/1378.66	77%	1378	n.a.	63	251
A-G2-CD	$C_{152}H_{211}N_{29}O_{26}$/2860.48	61%	2860	n.a.	70	247
A-G2.5-CD	$C_{164}H_{221}N_{31}O_{29}$/3090.70	53%	3091	n.a.	80	265
A-G3-CD	$C_{332}H_{455}N_{65}O_{58}$/6284.57	24%	6285	n.a.	75	224

[a] Determined by MALDI-TOF MS. [b] Second heating scan of DSC traces, with a heating rate of 10 °C min^{-1} in nitrogen. [c] 5% weight loss recorded by TGA at a heating rate of 10 °C min^{-1}. [d] Not detectable.

generation of dendron increased to a certain extent.[33] The effect of dendron generation on the T_gs of the dendrons D-G(X)-CD and A-G(X)-CD was similar to that of the dendrons A-G(X)-DR1. In addition, the alternating moiety-containing dendrons based on IDD (D-G(X)-CD) or IPDA (A-G(X)-CD) showed lower T_gs than the DR1-containing dendrons based on IPDA (A-G(X)-DR1). The presence of the long alkyl chain C18 groups in between the DR1 chromophores would bring about the reduced T_gs of dendrons. Furthermore, the T_gs of the dendrons D-G(X)-CD were lower than those of the dendrons A-G(X)-CD, except the T_g of D-G1-CD. This might be due to the fact that the presence of the methylene group in IDD reduced the rigidity of the dendron. On the other hand, the T_d values of the dendrons ranged from 205 to 279 °C. The dendrons with integer generation showed lower T_ds than did the dendrons with non-integer generation. This is

Table 2 Solubility of the NLO-active dendrons

Dendrons[a]	DMAc[c]	DMF[d]	DMSO[e]	1,4-Dioxane	THF[f]	Acetone
A-G1-DR1	+ +[b]	+ +	+ +	+ +	+ +	+ +
A-G1.5-DR1	+ +	+ +	+ +	+ +	+ +	+ +
A-G2-DR1	+ +	+ +	+ +	+ +	+ +	− −[b]
A-G2.5-DR1	+ +	+ +	+ +	+ +	+ +	+ +
A-G3-DR1	+ +	+ +	+ +	+ +	+ +	− −
D-G1-CD	+ +	+ +	+ +	+ +	+ +	+ −[b]
D-G1.5-CD	+ +	+ +	+ +	+ +	+ +	+ +
D-G2-CD	+ +	+ +	+ +	+ +	+ +	+ −
D-G2.5-CD	+ +	+ +	+ +	+ +	+ +	+ +
D-G3-CD	+ +	+ +	+ +	+ +	+ +	+ −
A-G1-CD	+ +	+ +	+ +	+ +	+ +	+ −
A-G1.5-CD	+ +	+ +	+ +	+ +	+ +	+ +
A-G2-CD	+ +	+ +	+ +	+ +	+ +	+ −
A-G2.5-CD	+ +	+ +	+ +	+ +	+ +	+ +
A-G3-CD	+ +	+ +	+ +	+ +	+ +	+ −

[a] Qualitative solubility was determined with 10 mg of polymer in 1 mL of solvent. [b] + +, soluble at room temperature; + −, partially soluble; − −, insoluble. [c] DMAc: *N*,*N*-dimethylacetamide. [d] DMF: *N*,*N*-dimethylformamide. [e] DMSO: dimethyl sulfoxide. [f] THF: tetrahydrofuran.

Table 3 Composition and *d* spacings of the NLO-active dendron intercalated MMTs

Samples	Intercalation agent	Dendron/MMT[a] (w/w)	Dendron/MMT[b] (w/w)	*d*-Spacing[c] (Å)
A-G1-DR1-M	A-G1-DR1	59/41	59/41	52
A-G2-DR1-M	A-G2-DR1	77/23	79/21	Featureless
A-G3-DR1-M	A-G3-DR1	89/11	85/15	Featureless
D-G1-CD-M	D-G1-CD	61/39	67/33	57
D-G2-CD-M	D-G2-CD	80/20	80/20	76
D-G3-CD-M	D-G3-CD	87/13	87/13	Featureless
A-G1-CD-M	A-G1-CD	58/42	63/37	48
A-G2-CD-M	A-G2-CD	78/22	80/20	73
A-G3-CD-M	A-G3-CD	88/12	87/13	Featureless

[a] Weight ratios of dendron and MMT were calculated based on the CEC: $X \times 1.2 \times 10^{-3} \times$ (molar mass of dendron) $= Y$, where X is the pristine weight of the clay, and Y is the weight of the dendron. The theoretical dendron ratio is given by $Y/(X + Y)$. [b] Weight ratios of dendron and MMT were calculated based on the results of TGA measurement in air. [c] Determined by X-ray diffraction patterns according to Bragg's equation ($n\lambda = 2d\sin\theta$).

attributed to the presence of the amino group at the focal site for the dendrons with integer generation. The lower thermal stability of the amino group led to the lower T_ds of dendrons with integer generation. Moreover, dendrons D-G(X)-CD and A-G(X)-CD showed higher T_ds than did dendrons A-G(X)-DR1. Lower T_ds were observed for the dendrons A-G(X)-DR1 with higher DR1 content, which is attributed to the relatively low thermal stability of the azobenzene dye.

The solubility of the NLO-active dendrons is summarized in Table 2. These dendrons exhibited excellent solubility in polar solvents, including DMAc, DMF, DMSO, 1,4-dioxane, and THF, while most of the dendrons are partially soluble in acetone. The dendrons with non-integer generation exhibited better solubility in acetone than the dendrons with integer generation. This is because the dendrons with non-integer generation possessed azetidine-2,4-diones at the focal points. This might possibly inhibit close packing of chain segments and consequently reduce the inter-chain interactions to enhance solubility. In addition, the dendrons D-G(X)-CD and A-G(X)-CD showed better solubility in acetone than the dendrons A-G(X)-DR1, which is attributed to the presence of the flexible alkyl chains in between DR1 chromophores at the periphery.

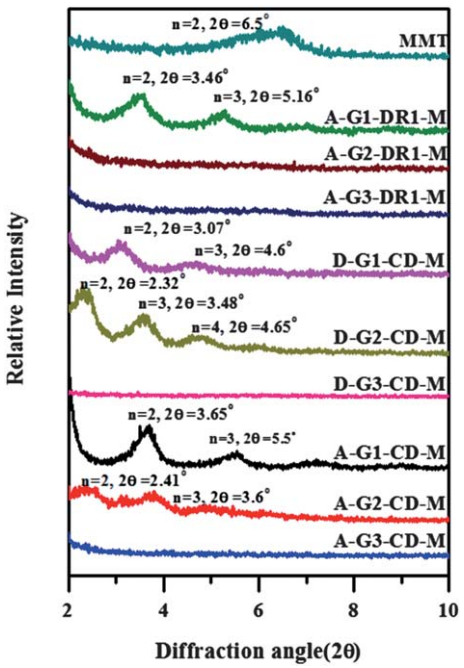

Fig. 2 XRD diffraction patterns of the dendron-intercalated MMTs.

3.2 Characterization of the NLO-active dendron intercalated MMTs

The NLO-active dendron intercalated MMTs (A-G(X)-DR1-M, D-G(X)-CD-M, and A-G(X)-CD-M; $X = 1$–3) were prepared by the intercalation of MMTs with IDD or IPDA based dendrons containing the peripheral groups of DR1 or alternating peripheral groups of C18/DR1 (A-G(X)-DR1, D-G(X)-CD, and A-G(X)-CD). The dendrons bearing secondary amines at the focal points could favorably participate in the ionic exchange process with MMTs. The compositions of the dendron intercalated MMTs are summarized in Table 3. The weight ratios of dendrons in MMTs calculated according to the CEC values were 59/41, 77/23,

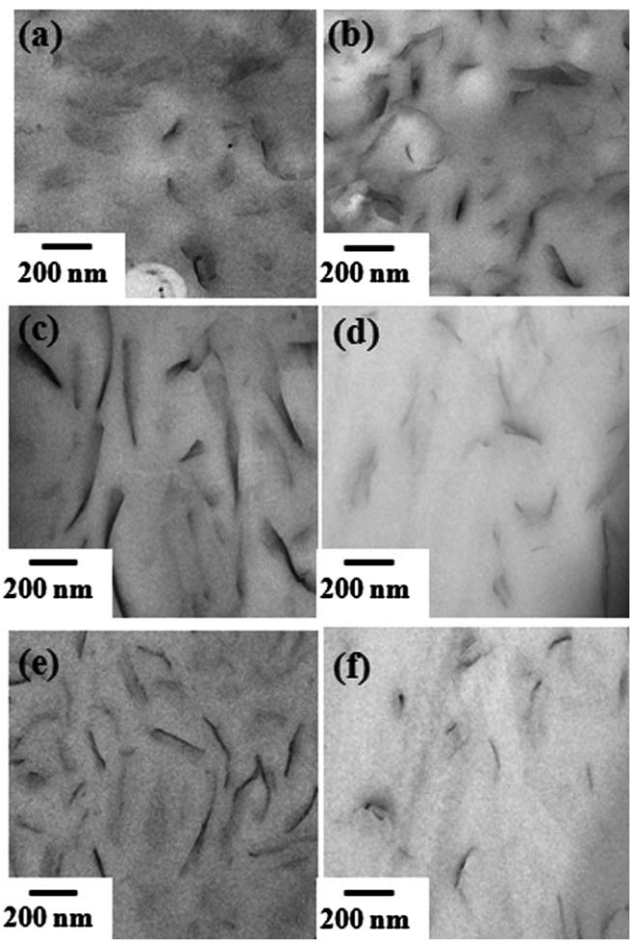

Fig. 3 TEM images of the dendron-intercalated MMTs ((a) A-G2.0-DR1-M, (b) A-G3.0-DR1-M, (c) D-G2.0-CD-M, (d) D-G3.0-CD-M, (e) A-G2.0-CD-M, and (f) A-G3.0-CD-M).

and 89/11 for A-G1-DR1-M, A-G2-DR1-M, and A-G3-DR1-M, respectively. Moreover, the weight ratios of dendrons in MMTs measured by TGA (air) were 59/41, 79/21, and 85/15, accordingly. The dendron contents in MMTs calculated according to the CEC values were similar to those measured by TGA. Moreover, the intercalated content of dendrons in MMTs increased when the dendrons of higher generation were intended for the dendron/MMT nanocomposites, A-G(*X*)-DR1-M. Similar results were observed for the NLO-active dendron intercalated MMTs such as D-G(*X*)-CD-M and A-G(*X*)-CD-M samples.

XRD patterns of the pristine MMT and dendron intercalated MMTs are shown in Fig. 2. The *d*-spacing values of the dendron/MMT nanocomposites are summarized in Table 3. The pristine MMT exhibited a diffraction band at a 2θ of 6.5°, indicating a *d*-spacing value of 13 Å. For the dendron/MMT nanocomposites, the *d*-spacing of A-G1-DR1-M based on Bragg's law ($n\lambda = 2d\sin\theta$ and the observed values for $n = 2$) was 52 Å, while no diffraction peak was found for A-G2-DR1-M and A-G3-DR1-M. This means that the *d*-spacings of the layered silicates were greater than 44 Å ($n = 1$, $2\theta < 6.5°$).[30] Apart from that, MMTs intercalated by dendrons A-G(*X*)-DR1 and D-G(*X*)-DR1 based on different building blocks exhibited similar interlayer *d*-spacings.[29,30] In addition, the *d*-spacings of D-G1-CD-M and D-G2-CD-M were 57 and 76 Å, respectively, while 48 and 73 Å for A-G1-CD-M and A-G2-CD-M, respectively. No diffraction peak was found for D-G3-CD-M and A-G3-CD-M. The XRD investigation revealed that the basal height was increased significantly as the dendritic molecule was anchored onto the silicate surface. Larger *d*-spacings were observed for the dendron/MMT nanocomposites as the dendrons with higher generation were utilized as the intercalating agents.

In order to confirm the results of the XRD study, TEM was utilized to visualize the spatial distribution of the dendron intercalated MMT samples (Fig. 3). Fig. 3(a) and (b) indicate that the layered silicates were exfoliated with dendrons A-G2-DR1 and A-G3-DR1, respectively. The featureless XRD patterns were observed for the A-G2-DR1-M and A-G3-DR1-M samples, while an intercalated morphology was observed for A-G1-DR1-M. In addition, the intercalated morphology was also observed for D-G2-CD-M and A-G2-CD-M (Fig. 3(c) and (e)). The basal spacing values measured from X-ray diffraction patterns were 73 and 76 Å for D-G2-CD-M and A-G2-CD-M, respectively. This demonstrates that the layered silicates were not completely exfoliated by either D-G2-CD or A-G2-CD. Similar intercalation results were also observed in our previous studies.[29,30] As shown in Fig. 3(d) and (f), TEM images indicate that the layered silicates were completely exfoliated by D-G3-CD and A-G3-CD, respectively. Therefore, the featureless XRD patterns were observed for D-G3-CD-M and A-G3-CD-M samples. Based on the above results, the dendrons A-G(*X*)-DR1 with all of the peripheral rigid chromophores were more ready and effective to intercalate the layered silicates as compared to the dendrons D-G(*X*)-CD and A-G(*X*)-CD with alternating peripheral groups of long alkyl chain C18 and DR1.

Table 4 Thermal and NLO properties of the nanocomposites based on the blend of NLO-active dendron intercalated MMT and PI

NLO-active nanocomposites[a]	Composition (dendron-MMT/PI)	Dendron-MMT content (wt%)	T_g[b] (°C)	Dye content (%)	r_{33}[c] (pm V^{-1})	r_{33}/dye content[d] (pm V^{-1})
D-G1.0-DR1-M-PI10	A-G1.0-DR1-M/PI	10	n.a.[e]	4.6	10.7	2.3
D-G1.0-DR1-M-PI20	A-G1.0-DR1-M/PI	20	193	9.2	14.3	1.5
D-G2.0-DR1-M-PI10	A-G2.0-DR1-M/PI	10	n.a.	3.6	9.9	2.7
D-G2.0-DR1-M-PI20	A-G2.0-DR1-M/PI	20	188	7.2	16.7	2.3
D-G3.0-DR1-M-PI10	A-G3.0-DR1-M/PI	10	n.a.	3.3	8.3	2.5
D-G3.0-DR1-M-PI20	A-G3.0-DR1-M/PI	20	150	6.5	13.9	2.1
A-G1.0-DR1-M-PI10	A-G1.0-DR1-M/PI	10	215	5.3	13.4	2.5
A-G1.0-DR1-M-PI20	A-G1.0-DR1-M/PI	20	208	10.5	18.8	1.8
A-G2.0-DR1-M-PI10	A-G2.0-DR1-M/PI	10	210	4.3	12.5	2.9
A-G2.0-DR1-M-PI20	A-G2.0-DR1-M/PI	20	191	8.5	22.7	2.7
A-G3.0-DR1-M-PI10	A-G3.0-DR1-M/PI	10	173	3.9	10.2	2.6
A-G3.0-DR1-M-PI20	A-G3.0-DR1-M/PI	20	150	7.8	17.9	2.3
D-G1.0-CD-M-PI10	D-G1.0-CD-M/PI	10	168	2.3	9.0	4.2
D-G1.0-CD-M-PI20	D-G1.0-CD-M/PI	20	135	4.6	14.0	3.0
D-G2.0-CD-M-PI10	D-G2.0-CD-M/PI	10	146	1.8	10.8	5.8
D-G2.0-CD-M-PI20	D-G2.0-CD-M/PI	20	130	3.7	18.5	5.0
D-G3.0-CD-M-PI10	D-G3.0-CD-M/PI	10	145	1.7	9.8	5.8
D-G3.0-CD-M-PI20	D-G3.0-CD-M/PI	20	106	3.3	17.2	5.2
A-G1.0-CD-M-PI10	A-G1.0-CD-M/PI	10	200	2.7	11.8	4.4
A-G1.0-CD-M-PI20	A-G1.0-CD-M/PI	20	202	5.5	16.5	3.0
A-G2.0-CD-M-PI10	A-G2.0-CD-M/PI	10	163	2.2	12.9	5.9
A-G2.0-CD-M-PI20	A-G2.0-CD-M/PI	20	160	4.4	22.4	5.1
A-G3.0-CD-M-PI10	A-G3.0-CD-M/PI	10	156	2.0	11.4	5.7
A-G3.0-CD-M-PI20	A-G3.0-CD-M/PI	20	150	4.0	19.0	4.8

[a] Nanocomposites comprising 10 wt% and 20 wt% of the dendron-modified clay with PI. [b] Second heating scan of DSC traces, with a heating rate of 10 °C min^{-1} in nitrogen. [c] EO coefficient without applying the poling process which was measured at 830 nm. [d] EO coefficient/dye content. [e] n.a.: not available.

3.3 Characterization of the NLO-active dendron intercalated MMT/PI nanocomposites

T_gs of the NLO-active dendron intercalated MMT/PI nanocomposites are summarized in Table 4. The T_g of the pristine polyimide was 270 °C. The T_gs of the nanocomposites A-G(X)-DR1-M/PI ranging from 150 to 215 °C were slightly higher than those of the nanocomposites D-G(X)-DR1-M/PI. The T_g decreased as the dendron intercalated MMT sample, D-G(X)-DR1-M or A-G(X)-DR1-M, was incorporated into the polyimide. Moreover, the T_gs of the nanocomposites comprising D-G(X)-CD-M or A-G(X)-CD-M ranging from 106 to 202 °C were much lower than that of the polyimide. This is because the dense packing of the polyimide chains was disrupted by the incorporation of the dendron intercalated MMTs. The decrease of T_g was more significant for the nanocomposite blended with a higher content of dendron intercalated MMTs. In addition, TGA thermograms of the dendron intercalated MMT/PI nanocomposites are shown in Fig S1 (ESI†). The T_d of the pristine polyimide was 516 °C. The thermal stability of the nanocomposites was poorer than that of the pristine polyimide due to the reason mentioned above. On the other hand, the distribution of the dendron intercalated MMTs in the polyimide was confirmed by the TEM investigation. TEM images of the nanocomposites D-G(X)-CD-M-PI10 (D-G(X)-CD-M/PI = 10 : 90 w/w) and D-G(X)-CD-M-PI20 (D-G(X)-CD-M/PI = 20 : 80 w/w) are shown in Fig. 4. The dendron intercalated MMTs D-G(X)-CD-M exhibited good dispersion in the polyimide matrices. Similar results were observed for the nanocomposites A-G(X)-DR1-M/PI and A-G(X)-CD-M/PI (as shown in Fig. S2 and S3, see ESI†). The morphologies of the dendron intercalated MMT/PI nanocomposites were further characterized by XRD. No diffraction peak was found for all of the dendron intercalated MMT/PI nanocomposites. This implies that MMTs were exfoliated when the organically modified MMTs were blended with the polyimide.

3.4 EO properties of the NLO-active dendron intercalated MMT/PI nanocomposites

As the NLO-active dendron intercalated MMT/PI nanocomposites were respectively solvent-casted onto the ITO glass substrate, no poling process was intended for aligning the NLO chromophores. A simple reflection technique was utilized to measure the EO coefficient (r_{33}) of the NLO-active thin films.[1,4] The unpoled NLO-active dendron intercalated MMT/PI nanocomposite samples were capable of exhibiting optical nonlinearity due to the ordered organization of NLO chromophores. According to the literature,[29,30] this phenomenon may be caused by the strong interaction force between the closely packed chromophore-containing dendritic structures, and the fixation of the dendritic structures on the silicate platelets in the same direction. Dye contents, r_{33} values, and r_{33}/dye content ratios of the dendron intercalated MMT/PI nanocomposites are summarized in Table 4. For the sake of highlighting the effectiveness in enhancing optical nonlinearity *via* the incorporation of alternating peripheral moieties onto the dendritic structures, the r_{33}/dye content ratios for the NLO-active nanocomposites are shown in Fig. 5. The dye contents of nanocomposites D-G(X)-DR1-M/PI and A-G(X)-DR1-M/PI were about two times as much as those of the corresponding D-G(X)-CD-M/PI and A-G(X)-CD-M/PI samples. Moreover, the dye contents of the D-G(X)-CD-M/PI samples were similar to those of the A-G(X)-CD-M/PI samples despite that these two series of samples are based on two different building blocks. Nevertheless, the r_{33} values of D-G(X)-CD-M/PI and A-G(X)-CD-M/PI with much lower dye contents were comparable to those of the D-G(X)-DR1-M/PI and A-G(X)-DR1-M/PI samples. Moreover, the r_{33} values of the nanocomposites comprising 20 wt% of dendron intercalated MMTs were higher than those of the nanocomposites comprising 10 wt% of dendron intercalated MMTs due to the presence of higher dye contents. On the other hand, the IPDA-based dendron intercalated MMT/PI nanocomposites (A-G(X)-DR1-M/PI) exhibited higher r_{33}/dye content ratios than those of the IDD-based dendron intercalated MMT/PI nanocomposites (D-G(X)-DR1-M/PI). This might be due to the fact that the building block IDD possessed a kinked methylene group between two phenyl rings. This could be somewhat detrimental for the NLO-active dendrons to be aligned in an acentric

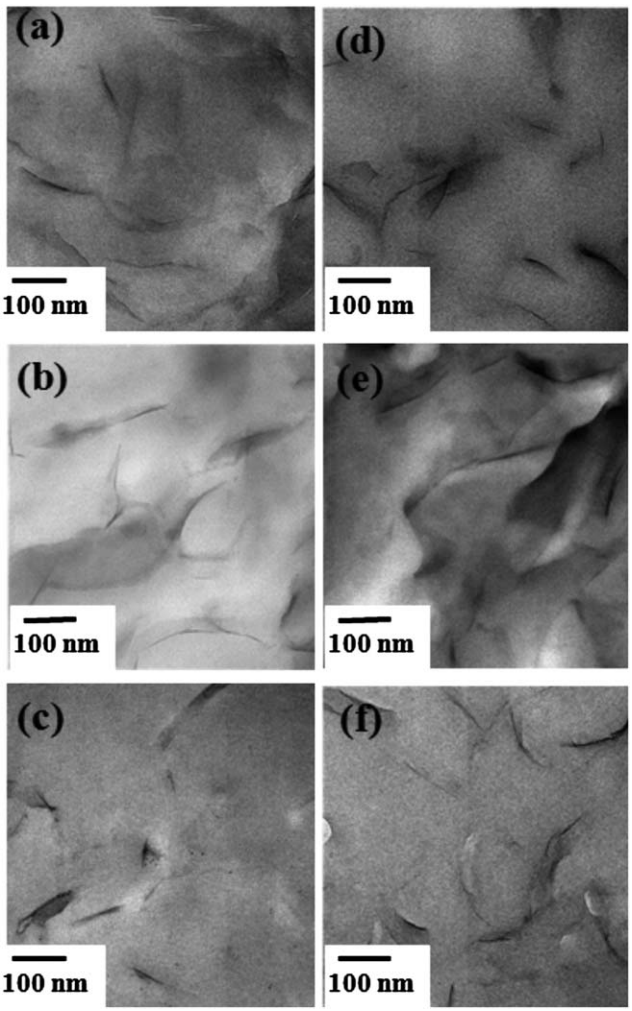

Fig. 4 TEM images of (a) D-G1-CD-M-PI10; (b) D-G2-CD-M-PI10; (c) D-G3-CD-M-PI10; (d) D-G1-CD-M-PI20; (e) D-G2-CD-M-PI20; and (f) D-G3-CD-M-PI20.

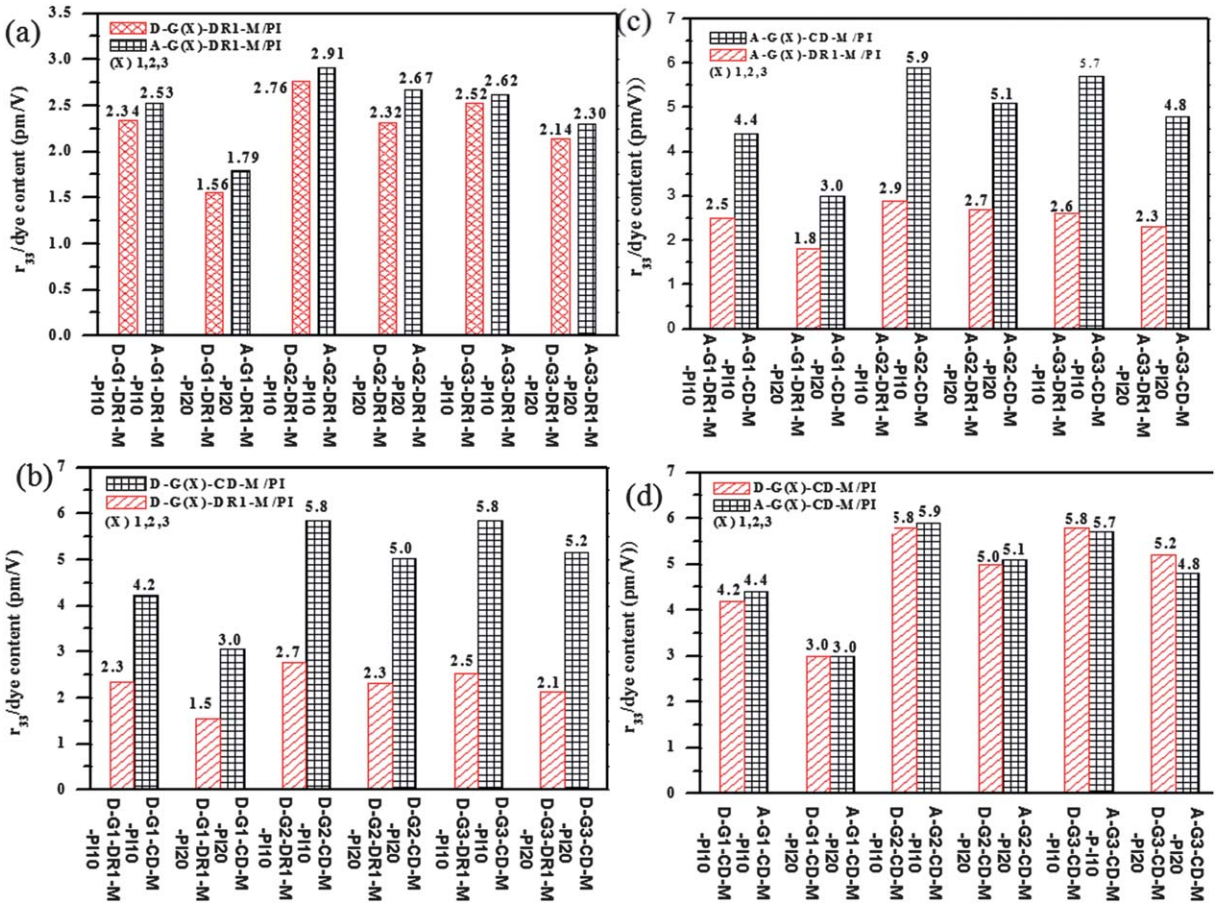

Fig. 5 EO coefficients for the chromophore-containing dendron intercalated MMT/PI nanocomposites comprising 10 wt% and 20 wt% of dendron-intercalated MMTs.

manner. Moreover, the r_{33}/dye content ratios of the D-G(*X*)-CD-M/PI and A-G(*X*)-CD-M/PI samples were about two times as large as those of the D-G(*X*)-DR1-M/PI and A-G(*X*)-DR1-M/PI samples. This indicates that the introduction of C18 groups as the hedges between the chromophores certainly enhanced the NLO properties of the resultant nanocomposites by minimizing the strong intermolecular dipole–dipole interactions among the chromophores. The C18 groups serving as hedges played an important role to improve electro-optical properties. In addition, higher r_{33}/dye content ratios were observed for the nanocomposites D-G2-CD-M/PI and D-G3-CD-M/PI as compared to those of the nanocomposites D-G1-CD-M/PI. Similar results were observed for the nanocomposites A-G(*X*)-CD-M/PI. This implies that the dendrons with higher generation or branching degree were favorable for the NLO chromophores to be efficiently aligned in an acentric manner. This is possibly due to a better ordered packing of chromophore-containing dendritic molecules contributed by the steric bulkiness of the dendritic structures. In contrast, it was more difficult to achieve the ordered arrangement of the dendrons with low branching degree due to the lack of steric bulkiness. However, this branching effect was not significant for the D-G(*X*)-DR1-M/PI and A-G(*X*)-DR1-M/PI samples. This is because the dipole–dipole repulsive interactions were present in these samples with the dendritic structures comprising all peripheral DR1 molecules. It is concluded that the r_{33}/dye content ratios are strongly dependent on the presence of dendrons with the alternating peripheral C18 and DR1 groups. Apart from that, the optical nonlinearity of DR1 in polyimide with the same chromophore density (10.5 wt%) was compared with that of A-G1.0-DR1-M-PI20. The r_{33} value of the dendron intercalated MMT/PI nanocomposite was larger than that of the electric-field poled polyimide based guest–host system (see ESI†).

In general, the EO coefficients of NLO polymers remain stable at low temperatures, but decay significantly at a specific temperature. This specific temperature is defined as the effective relaxation temperature (T_{ert}). To assess the ordered arrangement, T_{ert} is often utilized to determine the orientation of the dendron molecules and to further comprehend the ordered arrangement.[29] Two series of nanocomposites A-G(*X*)-DR1-M/PI and D-G(*X*)-CD-M/PI were selected to investigate their dynamic NLO thermal stability (Fig. 6). This is because the thermal stabilities of the A-G(*X*)-DR1-M/PI samples were similar to those of D-G(*X*)-DR1-M/PI. Moreover, the C18 hedging effect on the r_{33}/dye content ratios of the A-G(*X*)-CD-M/PI samples was similar to that of the D-G(*X*)-CD-M/PI samples. The IPDA based dendron intercalated MMT/PI nanocomposites A-G(*X*)-DR1-M-PI10 (A-G(*X*)-DR1-M/PI = 10 : 90 w/w; *X* = 1, 2, and 3) displayed T_{ert} values at 133, 115 and 101 °C, accordingly (Fig. 6(a)). Moreover, the T_{ert} values of the A-G(*X*)-DR1-M-PI20 samples

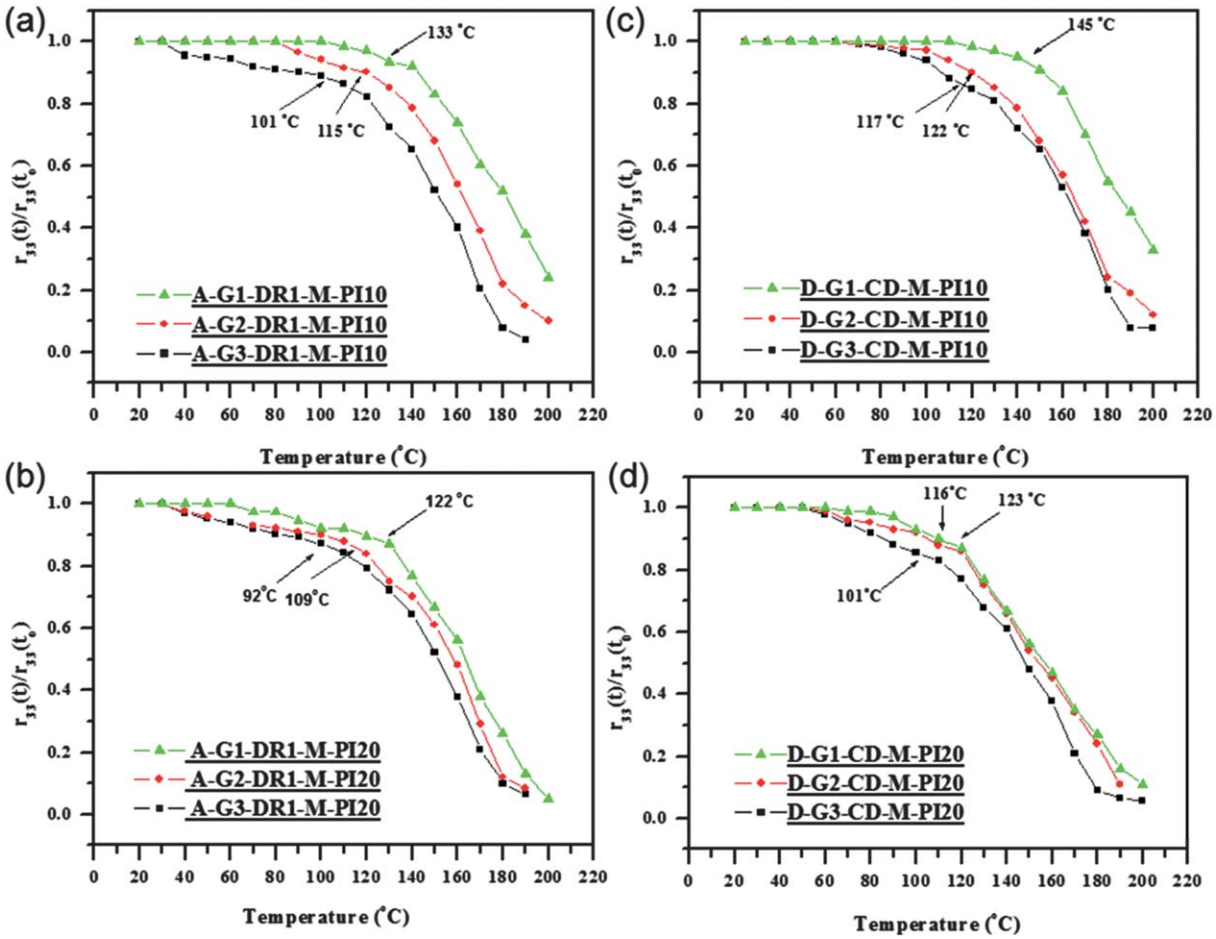

Fig. 6 Thermal dynamic properties of the DR1 dye containing dendron intercalated MMT/PI nanocomposites comprising 10 wt% and 20 wt% of dendron-intercalated MMTs: (a) A-G(*X*)-DR1-M-PI-10, (b) A-G(*X*)-DR1-M-PI-20, (c) D-G(*X*)-CD-M-PI-10, and (d) D-G(*X*)-CD-M-PI-20; where (*X*) = 1, 2, 3.

(A-G(*X*)-DR1-M/PI = 20 : 80 w/w; *X* = 1, 2, and 3) were about 122, 109 and 92 °C, respectively (Fig. 6(b)). The dynamic thermal stability was decreased for the A-G(*X*)-DR1-M/PI sample with increasing dendron generation. In fact, T_{ert} is closely related to the T_g of the measured sample. Consequently, the nanocomposite with a higher generation of dendrons would exhibit a lower T_g and T_{ert} according to the literature.[18,29,30] Moreover, the dynamic thermal stabilities of A-G(*X*)-DR1-M-PI20 samples were poorer than those of the A-G(*X*)-DR1-M-PI10 samples. This is because a higher content of the dendron intercalated MMTs in the polyimide would result in a lower T_g. In addition, as compared to the A-G(*X*)-DR1-M/PI samples, higher T_{ert} values were observed for the D-G(*X*)-CD-M/PI samples (Fig. 6(c) and (d)), especially for the D-G(*X*)-CD-M-PI10 samples, even though the T_gs of the D-G(*X*)-CD-M/PI samples were lower than those of the A-G(*X*)-DR1-M/PI samples. This is possibly due to the hedging effect of the peripheral C18 groups of NLO-active dendrons. The dendrons with the alternating functional groups (C18 and DR1) provided a fairly efficient way to prevent intermolecular electrostatic interactions at higher temperatures through the long alkyl chains as the hedges between chromophores. In other words, the presence of the C18 groups prevented the aggregation of the NLO chromophores when temperatures increased. This hedging effect was also observed for the D-G(*X*)-CD-M-PI20 samples.

The conformational change of the NLO-active nanocomposites at a certain relaxation temperature was studied by UV-vis spectroscopy. The changes of UV-vis spectra with time for D-G2-CD-M-PI10 after thermal treatment at 10 °C below T_{ert} for 1 h and cooling to room temperature or 92 °C are shown in Fig. 7. The absorption maxima of the nanocomposite thin film blue-shifted and the intensity decreased to a certain level after the thermal treatment. This phenomenon might be due to the self-association of the bulky dendrons to form intramolecular H-type aggregates, which is detrimental to NLO properties.[29,30,34] Due to the self-alignment nature, the original ordered arrangement is more stable than the H-type aggregates. Therefore, the H-type aggregates would relax to the original conformation after cooling down to 92 °C for a certain period of time. However, the H-type aggregates would recover to the original conformation in an extremely slow manner while cooling down to room temperature.[29,30,34] The conformational change of the thermal-treated dendron intercalated MMT/PI nanocomposites is illustrated in Fig. 8. When the annealing temperature was kept at 92 °C, the absorption maximum started to increase in a faster manner and came closer to its

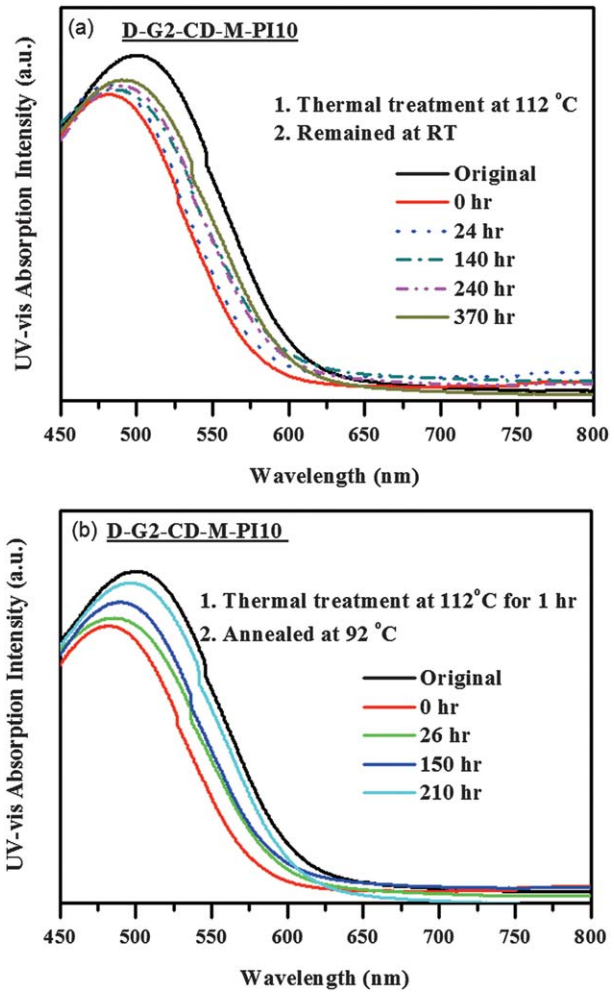

Fig. 7 UV-vis spectra of (a) D-G2-CD-M-PI10 after thermal treatment at 112 °C for 1 h and cooling to room temperature, and (b) D-G2-CD-M-PI20 after thermal treatment to 112 °C for 1 h and cooling to 92 °C.

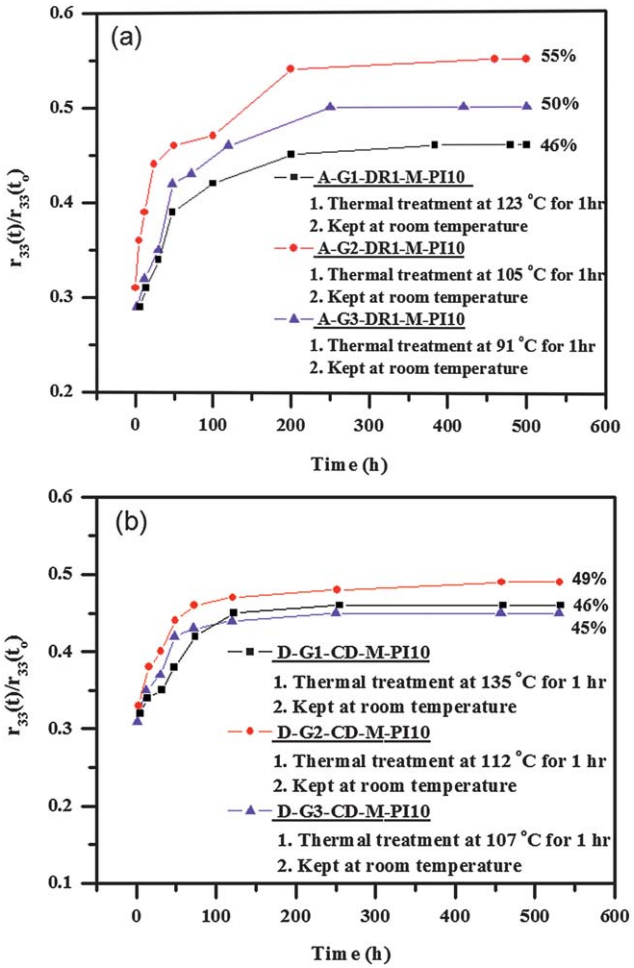

Fig. 9 Temporal behavior of EO coefficients for (a) A-G(*X*)-DR1-M-PI-10 and (b) D-G(*X*)-CD-M-PI-10 (*X* = 1–3).

original value. Similar results were observed for the rest of the NLO-active nanocomposites.

As mentioned earlier, the thermal treatment induced a drastic conformational change and influenced the ordered arrangement of the NLO chromophores. Moreover, the H-type aggregates would influence the ordered arrangement of NLO chromophores negatively. Therefore, the temporal behaviors of the EO coefficients ($r_{33}(t)/r_{33}(t_0)$) for the A-G(*X*)-DR1-M-PI10 and A-G(*X*)-CD-M-PI10 (A-G(*X*)-CD-M/PI = 10 : 90 w/w; *X* = 1, 2, and 3) samples after 1 h thermal treatment at 10 °C below T_{ert} were investigated (Fig. 9). Fig. 9(a) shows the temporal behavior of EO coefficients for the thermal-treated A-G1-DR1-M-PI10, A-G2-DR1-M-PI10, and A-G3-DR1-M-PI10 samples while the samples were maintained at room temperature. As the thermal-treated samples were respectively cooled from 123, 105, and 91 °C to room temperature, the r_{33} values of these three samples retained about 29, 31 and 29% of their original values, accordingly. The r_{33} values started to increase in a slow manner at the initial stage of 200 h. They only reached approximately 46–55% of their original values for a long period of time (500 h). In addition, similar temporal behaviors of the EO coefficients for the D-G(*X*)-CD-M-PI10 samples were observed in comparison with those for the A-G(*X*)-DR1-M-PI10 samples (Fig. 9(b)). As the thermal-treated samples were respectively cooled from 135, 112, and 107 °C to room temperature, the r_{33} values of these three samples retained about 32, 33 and 31% of their original values, accordingly. After the thermal-treated samples were kept at room temperature for 500 h, the r_{33} values of D-G1-CD-M-PI10, D-G2-CD-M-PI10, and D-G3-CD-M-PI10 recovered to about 46, 49, and 45% of their original values, respectively. The randomized chromophores of the D-G(*X*)-CD-M-PI10 samples recuperated more quickly toward the original ordered conformation as compared to those of the A-G(*X*)-DR1-M-PI10 samples. For the D-G(*X*)-CD-M-PI10 samples, it took only 100 h for

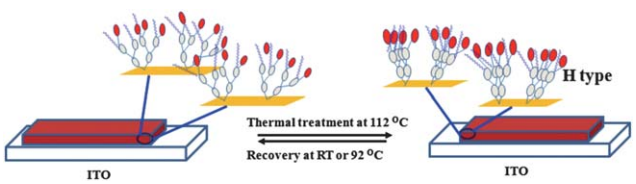

Fig. 8 Illustration of the conformational change of the thermal-treated dendron-intercalated MMT/PI nanocomposites.

the r_{33} values to recover to their maximum values at room temperature. On the other hand, it took 200 h for the r_{33} values of the A-G(X)-DR1-M-PI10 samples to reach their maximum values. This might be due to the presence of the long alkyl chains C18 between the DR1 chromophores in the D-G(X)-CD-M-PI10 samples. The dilution effect of the C18 groups at the periphery of the dendron favored the recovery of DR1 chromophores from the H-type aggregates to the original ordered conformation.

In order to study the annealing effect on the ordered arrangement of the NLO chromophores, the temporal behaviors of the EO coefficients for the thermal-treated A-G(X)-DR1-M-PI10 and D-G(X)-CD-M-PI10 (X = 1, 2, and 3) samples were investigated while the samples were kept at 30 °C below T_{ert} (Fig. 10). The r_{33} value started to increase in a relatively fast manner for the A-G(X)-DR1-M-PI10 and D-G(X)-CD-M-PI10 samples at the annealing temperature. The r_{33} values of the A-G(X)-DR1-M-PI10 and D-G(X)-CD-M-PI10 (X = 1, 2, and 3) samples could reach approximately 80% of their original values after 100 h. The recovery ratios were almost the same for the samples incorporated with different generations of dendrons. Unlike the thermal-treated samples kept at room temperature, the temporal behaviors of the A-G(X)-DR1-M-PI10 and D-G(X)-CD-M-PI10 samples are similar when annealed at 30 °C below T_{ert}. As the annealing temperature was close to T_{ert}, the influence of the dendrons with alternating peripheral groups of C18 and DR1 on the recovery of ordered morphology was not remarkable. On the basis of the above observation, the annealing temperature does play a critical role in reversing disordered morphology back to the original self-organized arrangement. To some extent, the closer the annealing temperature is to T_{ert}, the greater the NLO recovery ratio can be attained.

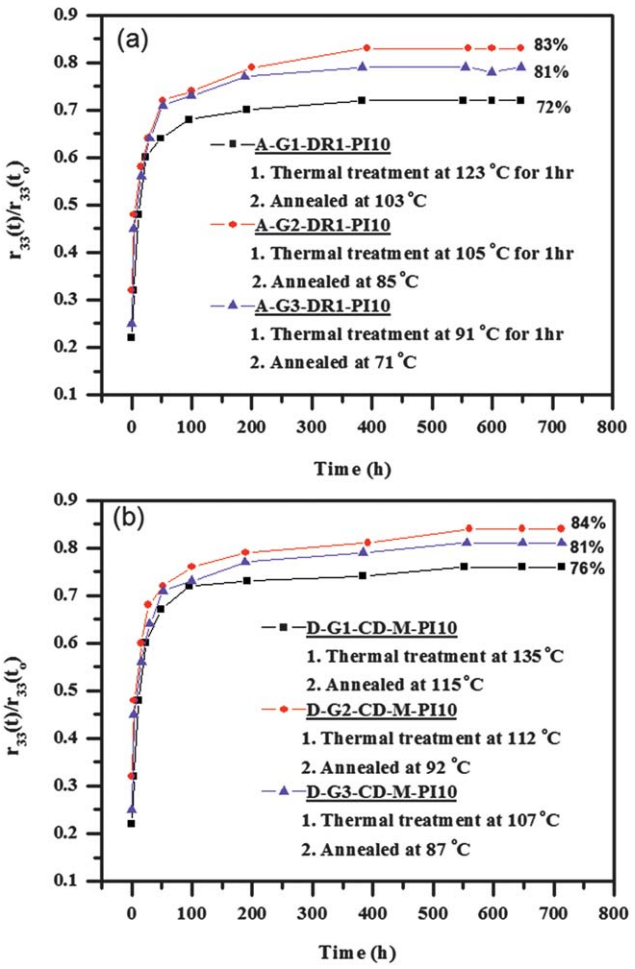

Fig. 10 Temporal behavior of EO coefficients for (a) A-G(X)-DR1-M-PI-10 and (b) D-G(X)-CD-M-PI-10 (X = 1–3).

4 Conclusion

A series of novel NLO-active dendrons with alternating peripheral C18 groups and DR1 molecules were synthesized in this work. Subsequently, MMTs were successfully intercalated with these chromophore-containing dendrons. The steric bulkiness of the dendrons and the interaction between the layered silicates and ITO glass substrates along with the polyimide brought about the exfoliated morphology, leading to ordered arrangement without applying the poling process.[29,30] The unpoled dendron-intercalated MMT/PI nanocomposite samples were capable of exhibiting r_{33} values of 9–22 pm V^{-1} because of the presence of an ordered morphology. The EO coefficient and NLO temporal stability were strongly affected by the presence of the dendrons with alternating C18 groups and DR1 molecules for these nanocomposites. The r_{33}/dye content ratios of the nanocomposites based on the dendrons containing the alternating peripheral groups were about two times as much as those of nanocomposites based on the dendrons containing all DR1 molecules at the periphery. Moreover, the thermal-treated nanocomposites based on the dendrons comprising the alternating peripheral groups recuperated more quickly to their original conformation as compared to the thermal-treated nanocomposites based on the dendrons with all peripheral DR1 molecules. The hedging effect of the peripheral C18 groups plays an important role of preventing dipole–dipole interactions among the chromophores, which is favorable for the formation of a more ordered morphology.

Acknowledgements

We thank National Science Council of Taiwan for financial support.

References

1 L. R. Dalton, *Adv. Polym. Sci.*, 2002, **158**, 1.
2 C. Samyn, T. Verbiest and A. Persoons, *Macromol. Rapid Commun.*, 2000, **21**, 1.
3 R. J. Jeng, C. C. Chang, C. P. Chen, C. T. Chen and W. C. Su, *Polymer*, 2003, **44**, 143.
4 C. C. Chang, C. P. Chen, C. C. Chou, W. J. Kuo and R. J. Jeng, *J. Macromol. Sci., Polym. Rev.*, 2005, **45**, 125.
5 H. L. Chang, H. L. Lin, Y. C. Wang, S. H. A. Dai, W. C. Su and R. J. Jeng, *Polymer*, 2007, **48**, 2046.
6 Z. Li, Z. Li, C. Di, Z. Zhu, Q. Li, Q. Zeng, K. Zhang, Y. Liu, C. Ye and J. Qin, *Macromolecules*, 2006, **39**, 6951.

7 Z. Li, W. Wu, G. Yu, Y. Liu, C. Ye, J. Qin and Z. Li, *ACS Appl. Mater. Interfaces*, 2009, **1**, 856.
8 Z. Shi, J. Luo, S. Huang, B. M. Polishak, X. H. Zhou, S. Liff, T. R. Younkin, B. A. Block and A. K. Y. Jen, *J. Mater. Chem.*, 2012, **22**, 951.
9 Z. Li, Q. Li and J. Qin, *Polym. Chem.*, 2011, **2**, 2723.
10 L. R. Dalton, P. A. Sullivan and D. H. Bale, *Chem. Rev.*, 2010, **110**, 25.
11 Z. Li, P. Hu, G. Yu, W. Zhang, Z. Jiang, Y. Liu, C. Ye, J. Qin and Z. Li, *Phys. Chem. Chem. Phys.*, 2009, **11**, 1220.
12 B. Kolli, A. P. Mishra, M. P. Joshi, S. R. Mohan, T. S. Dhami and A. B. Samui, *J. Polym. Sci., Part A: Polym. Chem.*, 2012, **50**, 1572.
13 H. Ma and A. K. Y. Jen, *Adv. Mater.*, 2001, **13**, 1201.
14 Y. Tian, C. Y. Chen, M. A. Haller, N. M. Tucker, J. W. Ka, J. Luo, S. Huang and A. K. Y. Jen, *Macromolecules*, 2007, **40**, 97.
15 M. J. Cho, D. H. Choi, P. A. Sullivan, A. J. P. Akelaitis and L. R. Dalton, *Prog. Polym. Sci.*, 2008, **33**, 1013.
16 J. Y. Do and J. J. Ju, *Macromol. Chem. Phys.*, 2005, **206**, 1326.
17 Z. Li, G. Yu, W. Wu, Y. Liu, C. Ye, J. Qin and Z. Li, *Macromolecules*, 2009, **42**, 3864.
18 Y. C. Chen, H. L. Chang, R. H. Lee, S. A. Dai, W. C. Su and R. J. Jeng, *Polym. Adv. Technol.*, 2009, **20**, 493.
19 Y. Wang, X. Wang, Y. Guo, Z. Cui, Q. Lin, W. Yu, L. Liu, L. Xu, D. Zhang and B. Yang, *Langmuir*, 2004, **20**, 8952.
20 Y. Wang, C. Wang, X. Wang, Y. Guo, B. Xie, Z. Cui, L. Liu, L. Xu, D. Zhang and B. Yang, *Chem. Mater.*, 2005, **17**, 1265.
21 A. Facchetti, L. Beverina, M. E. Van der Boom, P. Dutta, G. Evmenenko, A. D. Shukla, C. E. Stern, G. A. Pagani and T. J. Marks, *J. Am. Chem. Soc.*, 2006, **128**, 2142.
22 H. Kang, G. Evmenenko, P. Dutta, K. Clays, K. Song and T. J. Marks, *J. Am. Chem. Soc.*, 2006, **128**, 6194.
23 J. J. Lin, I. J. Cheng, R. Wang and R. J. Lee, *Macromolecules*, 2001, **34**, 8832.
24 C. C. Chou, F. S. Shieu and J. J. Lin, *Macromolecules*, 2003, **36**, 2187.
25 J. J. Lin, C. C. Chu, M. L. Chiang and W. C. Tsai, *Adv. Mater.*, 2006, **18**, 3248.
26 G. W. Beall and M. Goss, *Appl. Clay Sci.*, 2004, **27**, 179.
27 J. J. Lin, I. J. Chen and C. C. Chou, *Macromol. Rapid Commun.*, 2003, **24**, 492.
28 M. A. Osman, M. Ploetze and P. Skrabal, *J. Phys. Chem. B*, 2004, **108**, 2580.
29 Y. C. Chen, T. Y. Juang, S. A. Dai, T. M. Wu, J. J. Lin and R. J. Jeng, *Macromol. Rapid Commun.*, 2008, **29**, 587.
30 Y. C. Chen, T. Y. Juang, T. M. Wu, S. A. Dai, W. J. Kuo, Y. L. Liu, F. M. C. Chen and R. J. Jeng, *ACS Appl. Mater. Interfaces*, 2009, **1**, 2371.
31 C. C. Chang, T. Y. Juang, W. H. Ting, M. S. Lin, C. M. Yeh, S. A. Dai, S. Y. Suen, Y. L. Liu and R. J. Jeng, *Mater. Chem. Phys.*, 2011, **28**, 157.
32 S. M. Shau, C. C. Chang, C. H. Lo, Y. C. Chen, T. Y. Juang, S. A. Dai, R. H. Lee and R. J. Jeng, *ACS Appl. Mater. Interfaces*, 2012, **4**, 1897.
33 C. C. Tsai, T. Y. Juang, S. A. Dai, T. M. Wu, W. C. Su, Y. L. Liu and R. J. Jeng, *J. Mater. Chem.*, 2006, **16**, 2056.
34 E. H. A. Beckers, S. C. J. Meskers, A. P. H. J. Schenning, Z. J. Chen, F. Wurthner, P. Marsal, D. Beljonne, J. Cornil and R. A. J. Janssen, *J. Am. Chem. Soc.*, 2006, **128**, 649.